WAVE ATTENUATION EFFECTS BY MANGROVES USING THREE-DIMENSIONAL NUMERICAL CALCULATIONS

Mei Yoshida[1], Hinano Ohara[1], Yota Enomoto[1] and Taro Arikawa[2]

Mangroves significantly attenuate tsunami wave heights, and recent studies have explored this using both experiments and numerical simulations. Fluid behavior in mangrove forests is highly three-dimensional and requires high computational cost for numerical analysis. Therefore, this study employs a simplified modeling method using the Dupuit-Forchheimer law, which reproduces attenuation effects with low computational cost. Results show that wave height attenuation was consistent with experiments even at coarse grid resolutions (2–4 times the trunk diameter). Local scale calculations confirmed that wider mangrove forests and higher resistance coefficients reduce transmissivity, aligning with experimental and prior research trends. This approach demonstrated potential for evaluating mangrove-based disaster mitigation.

Keywords: mangrove; green infrastructure; numerical modeling; Dupuit-Forchheimer law

Introduction

Green infrastructure is a national and regional sustainable development approach that aims to utilize the functions of the natural environment to solve various problems in society. During the 2004 Sumatra earthquake and Indian Ocean tsunami, a tsunami triggered by a magnitude 9.3 earthquake caused devastating damage, but the tsunami energy attenuation effect of mangrove forests was observed (Yanagisawa et al., 2007). Since then, mangrove forests have garnered attention as a natural defense mechanism protecting coastal areas from tsunami disasters. The tsunami attenuation effects of mangroves are widely recognized through field surveys following disasters (Yanagisawa et al., 2010), and recent research has focused on both experimental and numerical approaches.

For mangroves with complex prop-root geometries, actual mangroves were measured and modelled using a 3D scanner, and hydraulic model experiments were conducted using models created by a 3D printer (Chang et al., 2019). Furthermore, two-dimensional wide-area simulations using energy balance equations such as the SWAN model have also been used to analyze wave attenuation effects (Reinout et al., 2010). The wave attenuation effect of mangroves was demonstrated through hydraulic model experiments and numerical simulations (Yanagisawa et al. 2005). They stated that it is important to accurately estimate the drag force of mangrove forests in numerical simulations and examined the drag force based on the results of experiments and simulations.

On the other hand, developing a versatile model applicable to various wave conditions, including surf zones, requires three-dimensional calculations. However, detailed vegetation reproduction requires a grid resolution that can solve the complex shapes of trunk and leaves, which increases the computational cost, necessitating the development of cost-effective simulation methods. For instance, Tadokoro et al. (2021) utilized CADMAS-SURF/3D (CS3D) (Arikawa et al., 2005) to perform investigations of wave height attenuation effects by assigning porosity and drag coefficient to porous medias modeled as mangroves. However, since the resistance force in this method depends on grid resolution, achieving accurate calculations requires a sufficiently fine grid resolution. While this approach is feasible at experimental scales, it presents challenges for wide-area simulations.

Therefore, under current computational constraints, it is crucial to establish methods that allow wide-area simulations of coastal vegetation with complex root structures that are independent of grid resolution. Yoshida et al. (2023) simplified mangrove modeling using porosity and adopted the Dupuit-Forchheimer (DF) law, which allows resistance force calculations independent of grid resolution. Through sensitivity analyses of the resistance coefficients α_0 and β_0 for materials constituting porous medias, they demonstrated that appropriate parameter settings yield reasonable results even with grid resolutions approximately four times the mangrove trunk diameter.

Given the challenges identified in previous studies, the following objectives were pursued to examine numerical modeling methods for mangroves and their attenuation effects:

1. Investigate wave height attenuation effect and the validity of the modeling method by comparing existing experiments with replicated calculations in which the DF law is applied to mangrove modeling.
2. Perform local scale adaptive simulations using modeling method which DF law is applied, evaluating its applicability and attenuation effects, as well as the influence of mangrove forest width in the offshore direction on long-period waves.

[1] Civil, Human and Environmental Engineering Course of Graduate School of Science and Engineering, Chuo University, 1-13-27 Kasuga, Bunkyo-ku, Tokyo, 112-8551, Japan

[2] Department of Civil and Environmental Engineering, Chuo University, 1-13-27 Kasuga, Bunkyo-ku, Tokyo, 112-8551, Japan

Method

In this study, CS3D which a three-dimensional calculation model based on the continuity equation (Equation 1) and the extended Navier-Stokes equations based on porous media (Equation 2: Only in x direction due to limitation) was used.

$$\frac{\partial \gamma_x u}{\partial x} + \frac{\partial \gamma_y v}{\partial y} + \frac{\partial \gamma_z w}{\partial z} = \gamma_V S_\rho \tag{1}$$

$$\begin{aligned} \lambda_v \frac{\partial u}{\partial t} + \frac{\partial \lambda_x uu}{\partial x} + \frac{\partial \lambda_y vu}{\partial y} + \frac{\partial \lambda_z wu}{\partial z} = & -\frac{\gamma_v}{\rho}\frac{\partial p}{\partial x} + \frac{\partial}{\partial x}\left\{\gamma_x \nu_e \left(2\frac{\partial u}{\partial x}\right)\right\} \\ & + \frac{\partial}{\partial y}\left\{\gamma_y \nu_e \left(\frac{\partial u}{\partial y} + \frac{\partial v}{\partial x}\right)\right\} + \frac{\partial}{\partial z}\left\{\gamma_z \nu_e \left(\frac{\partial u}{\partial z} + \frac{\partial w}{\partial x}\right)\right\} \\ & -\gamma_v D_x u - R_x + \gamma_v S_u \end{aligned} \tag{2}$$

Where t is time, x,y is horizontal coordinate, z is vertical coordinate, u, v, w is fluid velocity of x,y,z directions, ρ is density, p is pressure, ν_e is sum of kinematic viscosity of molecules ν and vortex viscosity ν_t, g is gravity acceleration, γ_v is porosity, $\gamma_x, \gamma_y, \gamma_z$ is surface transmission rate of x, y, z directions, D_x: coefficients for energy decay band, S_ρ, S_u is source term for wave sources, R_x is resistance from porous media. λ_v, λ_x, λ_y, λ_z are shown in eq.(3) using inertia coefficient C_M.

$$\left.\begin{aligned} \lambda_v &= \gamma_v + (1-\gamma_v)C_M \\ \lambda_x &= \gamma_x + (1-\gamma_x)C_M \\ \lambda_y &= \gamma_y + (1-\gamma_y)C_M \\ \lambda_z &= \gamma_z + (1-\gamma_z)C_M \end{aligned}\right\} \tag{3}$$

The resistance from the porous media R_x is expressed by Equations (4), with C_D as the resistance coefficient. CS3D allows the calculation on a variable grid with a fine grid around the structure, however to keep C_D/Δx constant, the value of C_D must be set appropriately according to the grid resolution.

$$R_x = \frac{1}{2}\frac{C_D}{\Delta x}(1-\gamma_x)u\sqrt{u^2+v^2+w^2} \tag{4}$$

Kotoura et al. (2010) introduced the DF law extended to three dimensions in CS3D and applied it to rubble structures and confirmed that highly accurate calculations are possible regardless of the grid resolution, wave conditions, and rubble grain size. Equations (5.1)-(5.3) for calculating the resistance force R_x are shown below.

$$R_x = \gamma_V(\gamma_V u)\left(\alpha + \beta\sqrt{(\gamma_x u)^2 + (\gamma_y u)^2 + (\gamma_z u)^2}\right) \tag{5-1}$$

$$\alpha = \alpha_0 \frac{(1-\gamma_V)^3}{{\gamma_V}^2}\frac{\nu}{d^2} \tag{5-2}$$

$$\beta = \beta_0 \frac{(1-\gamma_V)}{{\gamma_V}^3}\frac{1}{d} \tag{5-3}$$

Where α, β is coefficient, α_0, β_0 is resistance coefficient for materials, γ is kinematic viscosity coefficient, d is representative diameter.

The mangrove was assumed to be porous media, and the DF law was employed to model the system, with the resistance coefficient for materials. There is no established method for giving resistance coefficients and their evaluation when vegetation is used as a porous structure. In this study, the resistance coefficients α0 was set to 500, 1000, and 1500, and β0 to 0.35, 0.5, and 1.0, for a total of nine combinations. These values were determined with reference to the resistance coefficients of highly porous medias with similar shapes, as reported by Kondo and Takeda (1983). The representative diameter d used in the DF law was adopted as the Diameter at Breast Height (DBH) of mangroves (Kondo, 1981). This diameter corresponds to the height of 1.2–1.3 m from the base of the trunk. The porosity was set to 0.97, based on experimental condition, with its calculation considering only the trunk diameter.

The attenuation effect of tsunami wave heights passing through mangroves was quantitatively evaluated by defining the transmissivity. The transmissivity is calculated as

$$K_T = \frac{b}{a} \tag{6}$$

Where a is the maximum wave height in front of the mangroves, b is maximum wave height behind mangroves. Using, this method, the following sections provide comparisons with experimental data.

Experimental replication calculations

The numerical calculations in this study are reproductions of experiments conducted with reference to the 2018 Sulawesi earthquake conducted by Tadokoro et al. (2021). Figure 1 shows the experimental cross section and the shaded area representing the location of mangroves. For the vegetation model, roots, trunks, and branches of mangroves were reproduced using wire.

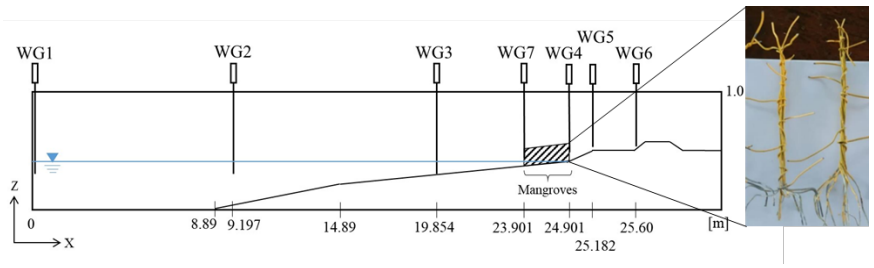

Figure 1. Experimental cross section and the vegetation model (Cited from Tadokoro et al. (2021))

The experiment conditions shown in Table 1.

Table 1. Experimental and calculated conditions (Cited from Tadokoro et al. (2021))

Water Depth (m)	Wave Height (m)	Mangrove Widths (m)
0.4 0.414 0.428	0.07, 0.09 0.056, 0.076, 0.096 0.07, 0.09	0 (Without), 0.4, 0.7, 1.0

Calculations were performed with the same cross section and wave making conditions as in the experiment. The solitary wave applied was generated using Equation (7).

$$\eta(x,t) = H sech^2\left(\sqrt{\frac{3H}{4h^2}}(x - \sqrt{g(h+H)}t)\right) \tag{7}$$

Where H is wave height and h is water depth.

A wave generation source was employed to satisfy the condition for non-reflective wave generation. To prevent wave reflection at the boundary in the negative x direction, the left end of the tank was used as an open boundary, the wave generation source are 30 m away from the wave making boundary.

A sensitivity analysis has been carried out with nine different combinations of α_0 and β_0. The grid sizes in x and y directions (Δx and Δy) were set to 1 cm and 2 cm, respectively, and z direction (Δz) was set to 1 cm in both cases to account for the number of wave height divisions. The diameter of the mangrove trunk was set to 5 mm based on DBH. The porosity was calculated from the experimental model and set at 0.97.

Figure 2 shows the comparison of time series water levels at WG1 between experimental and calculated value for the case without mangroves and Δx = 0.01m. The numerical results are in good agreement with the experiments in terms of arrival times, waveforms and maximum wave heights, demonstrating the validity of CS3D.

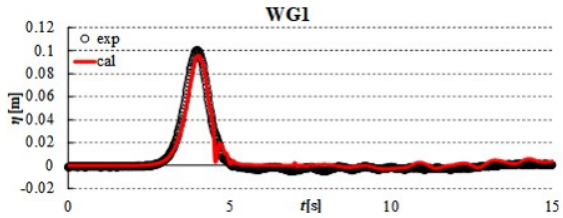

Figure 2. Comparison between experimental and calculated time series of water levels at WG1

Figure 3 shows the time series of water level fluctuation at WG7, located in front of the mangroves, and WG4, located behind the mangroves. In the numerical calculations, a phase lag was observed compared to the experimental values. While this discrepancy may be attributed to temporal shifts in the experimental data or numerical viscosity. Therefore, in this study, the phase lag is not considered, and the analysis focuses on wave heights instead.

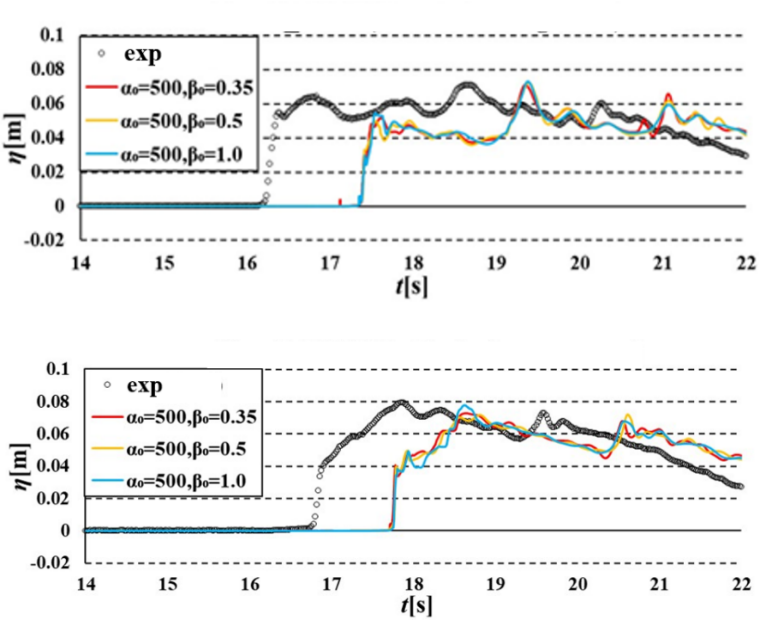

Figure 3. Comparison between experimental and calculated time series of water levels at WG7 (upper figure) and WG4(bottom figure)

Figure 4 shows the relationship between K_T and the wave height-to-water depth ratio at WG7 in front of the mangrove. The attenuation effect was reproduced with comparable accuracy even with a Δx and Δy grid size of 2 cm. The trend observed in the experiments, where K_T decreases as H/h increases, was reproduced. However, in numerical calculations, K_T were slightly overestimated compared to the experiment. This may be due to the effect of reflected waves from the terrain behind and coarser grid resolution.

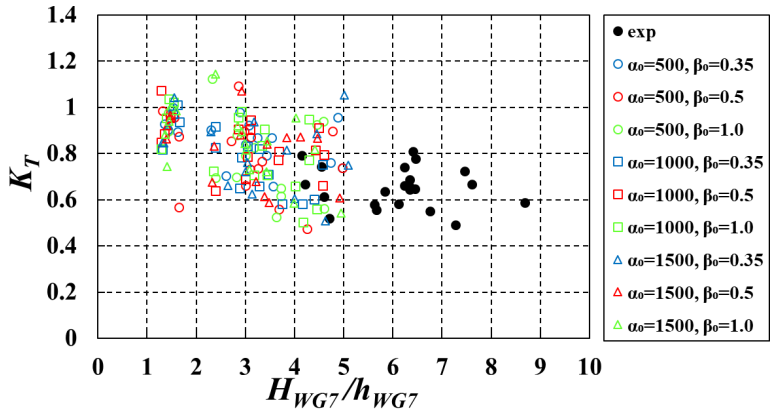

Figure 4. Relationship between K_T and *H/h*

Figure 5 shows the relationship between K_T and B/L. B/L is ratio of mangrove width to wavelength. The wavelength was calculated using the equation (8-1) and (8-2) based on the wave height at WG1, the wave generation point, and the initial water depth.

$$L = \frac{2\pi}{k} \tag{8-1}$$

$$k = \sqrt{\frac{3H_{wg1}}{4h_{WG1}^3}} \tag{8-2}$$

When organized in terms of the relation between K_T and B/L, the combination of the coefficients most consistent with the experiment in relation to K_T and B/L is α_0=1500, β_0=1.0. The experimental results indicate that a larger B/L ratio leads to a smaller K_T. However, this trend was not reproduced in the numerical simulations. This discrepancy suggests that the numerical model may not adequately capture the effects of local scale calculations with a larger B/L at larger scales. To address this, local scale calculations with a larger B/L are necessary to investigate the attenuation effect further.

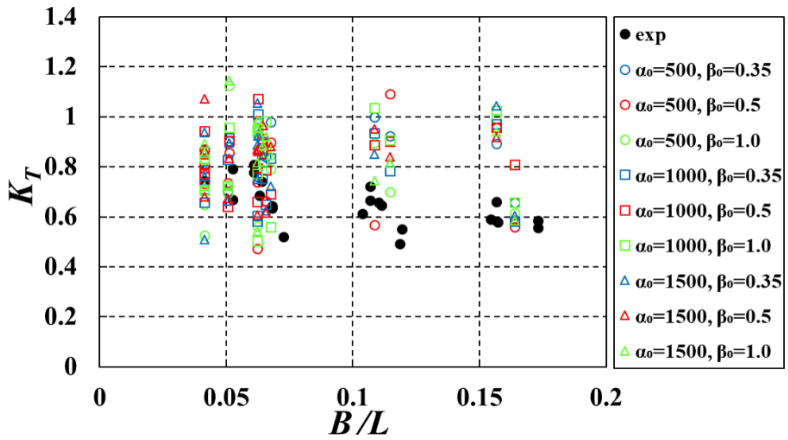

Figure 5. Relationship between K_T and B/L (Experimental replication calculations)

Local scale calculations

Based on the results of experimental reproduction calculations, local scale calculations were conducted with practical application in mind. Referring to the 2018 Sulawesi earthquake, the calculations used the cross-section shown in Figure 7, which was simplified from the topography west of Palu, Indonesia, as illustrated in Figure 6. The height of the elevated road behind the mangroves was set to 2.5

m, based on the Technical Report of the Domestic Support Committee on Tsunamis and Liquefaction-induced Landslides (Coastal Areas).

Table 2 summarizes the calculation conditions. The isolated wave with a height of 2.0 m and a period of 210 seconds was applied using a wave-generating source in water with a depth of 3.7 m. The mangrove widths were set to eight different values: 0, 20, 35, 50, 100, 150, 200, and 250 m. For the resistance coefficients, sensitivity analysis was performed using the same values as in the experimental reproduction calculations: α_0= 500,1000,1500 and β_0= 0.35,0.5,1.0. The grid size was set to Δx = 1.0 m to be approximately 3 times the diameter of the trunk.

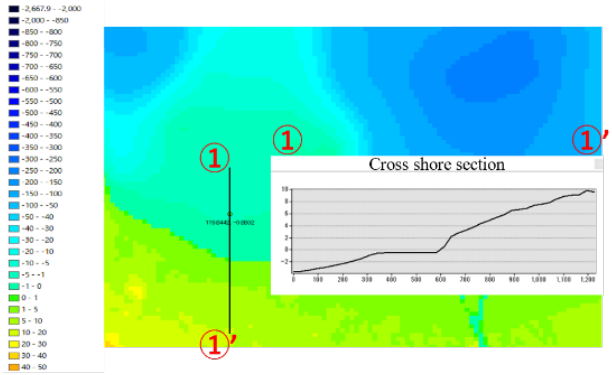

Figure 6. Cross section of the western part of Palu, Indonesia

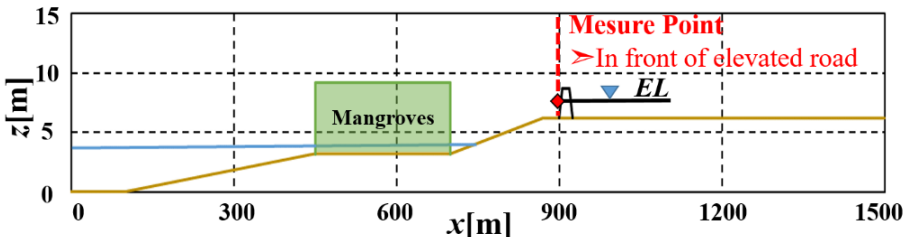

Figure 7. Calculated cross section

Table 2. calculated conditions		
Water Depth (m)	Wave Height (m)	Mangrove Widths (m)
3.7 (MSL+0.7)	2	0, 20, 35, 50, 100, 150, 200, 250

Figure 8 and figure 9 show the spatial wave height distribution illustrating the differences caused by the mangrove width for the same α_0 and β_0. Figure 8 represents the pattern with the minimum resistance coefficient, while figure 9 shows the pattern with the maximum.

For the smallest mangrove width of 20 m, the waveforms were nearly identical to those without mangroves, regardless of the combination of the resistance coefficients used, indicating minimal attenuation effect from the mangroves. Conversely, as the mangrove width increased, the attenuation effect became more apparent. For mangrove widths of 200 m and 250 m, the number of cases where waves overtopped the elevated road decreased regardless of the resistance coefficients applied.

These results suggest that when the mangrove width is small, the attenuation effect is limited, and significant differences based on the resistance coefficients are not reproduced. However, as the mangrove width increases, the attenuation effect becomes more pronounced, and variations in resistance due to different coefficients can be observed. Furthermore, the wave height distribution decreased as α_0 and β_0 increased, indicating that the resistance coefficients had a significant impact.

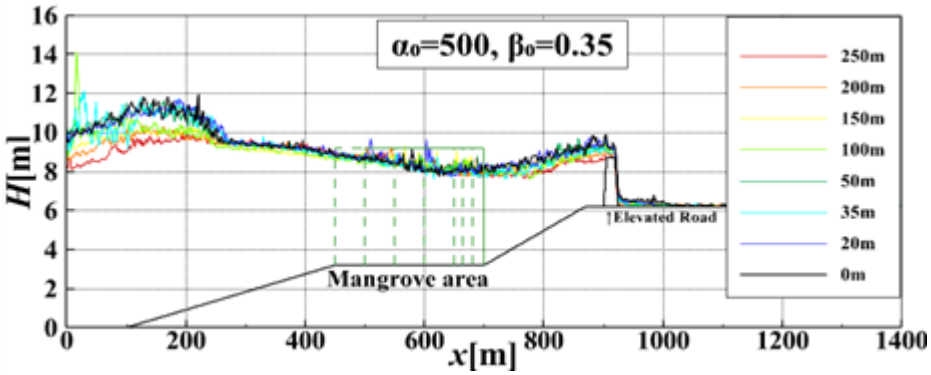

Figure 8. Calculated cross section

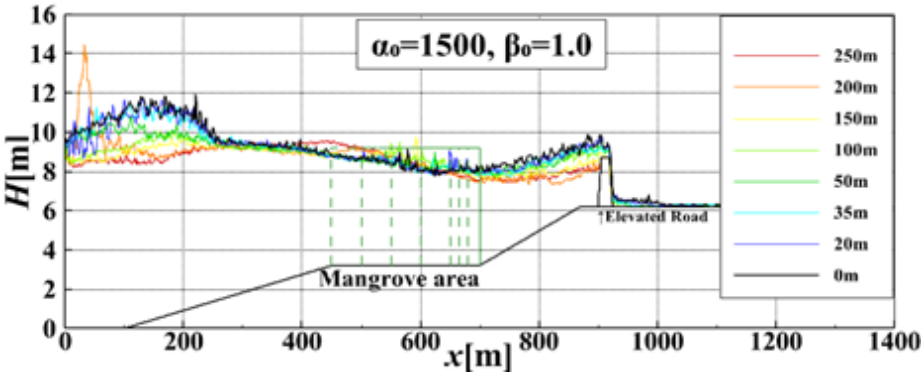

Figure 9. Calculated cross section

Figure 10 shows the relationship between run-up height and mangrove widths. Each plot represents the average of the results from nine combinations of α_0 and β_0 and shows their corresponding approximation lines. Overtopping occurs when the mangrove width is between 0 and 100 m, but is suppressed for widths of 150 m or more. For a width of 250 m, the run-up height is reduced by approximately 30% compared to the case without mangroves. Under the conditions of this study, these results suggest that a mangrove width of at least 150 m is desirable when planting mangroves as a disaster mitigation measure.

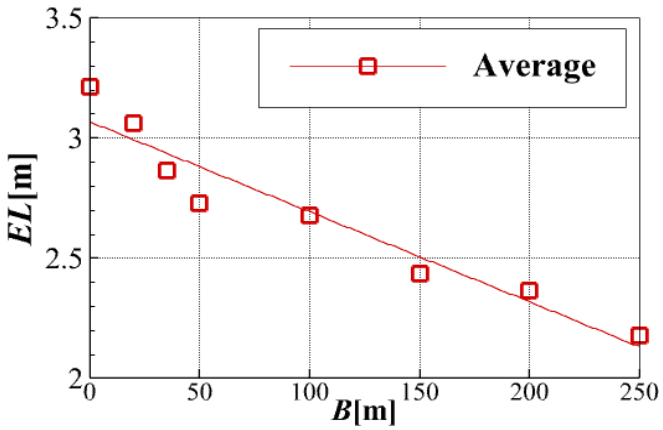

Figure 10. Relationship between run-up height and mangrove widths

Figure 11 shows the Relationship between K_T and B/L. The local scale calculations allow the study to be performed over a larger range of B than the experimental replication calculations. The trend that K_T becomes smaller as B/L increases is consistent with the experiments. Regarding the resistance coefficients, it was found that K_T decreases and attenuation is achieved regardless of α_0 when β_0=1.0. According to Equation (5-1), β_0 is the coefficient associated with the square of the flow velocity, suggesting that its influence becomes relatively significant under high flow velocity conditions. Moreover, it was shown that any combination of resistance coefficients could be reproduced within the range shown in the figure11.

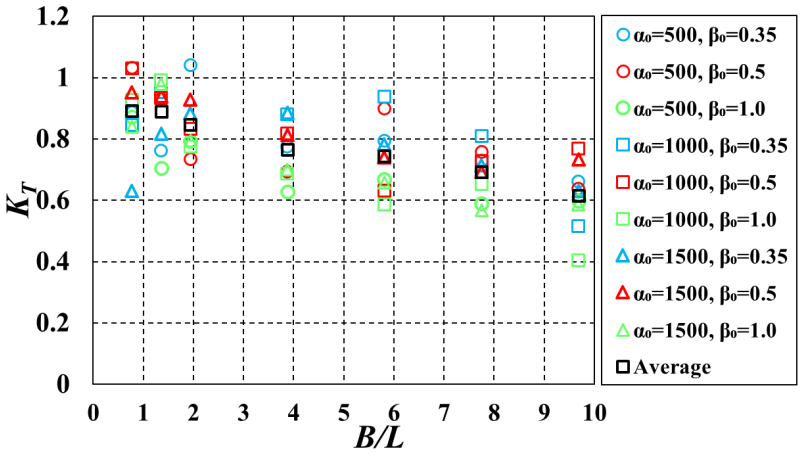

Figure 11. Relationship between K_T and B/L (local scale calculations)

Conclusion

This study employs a simplified modeling method using the DF law, which reproduces attenuation effects with low computational cost. The main conclusions derived from this study and future challenges are summarized below:

- The mangrove modeling method using the DF law successfully reproduced the attenuation effect. It was demonstrated that a grid resolution of approximately 2 to 4 times the trunk diameter did not significantly impact accuracy. Furthermore, consistent computational results were obtained using the specified resistance coefficients α_0 and β_0.
- In the experimental reproduction calculations, the relationship between K_T and H/h was consistent with the experimental data. Regarding B/L, while the experiments showed that attenuation increased as B/L grew, this trend was not observed in the numerical calculations. This discrepancy is likely due to the relatively small mangrove width compared to the wavelength.
- In the local scale calculations, greater mangrove widths and higher resistance coefficients resulted in more pronounced attenuation effects, and a reduction in run-up heights in front of the elevated road was observed. The relationship between K_T and B/L was consistent with the trends observed in experiments and previous studies.
- Since the present modeling method does not account for the complex roots, trunks, or branches of mangroves, future challenges include reflecting and reproducing the differences in resistance caused by these factors within the model.
- As mangroves predominantly inhabit surf zones, further detailed examination of wave-breaking attenuation is necessary. Additionally, mangrove forests are expected to contribute to coastal sand dune erosion prevention in addition to their tsunami attenuation effects. Elucidating the detailed mechanisms of these effects remains a future research topic.

REFERENCES

Arikawa, T., Yamada, F. and Akiyama, M.: Investigation of Applicability for Tsunami Wave Forces in a 3-D Numerical Wave Tank, Proceedings of Coastal Engineering, JSCE, Volume 52, pp. 46-50, 2005.

Chang, C. W., Mori, N., Tsuruta, N. and Suzuki, K.: Estimation of Wave Force Coefficients on Mangrove Models, *Journal of Japan Society of Civil Engineers, Ser. B2 (Coastal Engineering)*, Vol.75, Issue 2, pp. I_1105-I_1110, 2019.

Kondo, S. and Takeda, H., Dissipating structure, pp.70-129, Morikita Publishing Co., 1983.

Kondo, S., Hydraulic characteristics of upright wave dissipating structures, Collection of Lectures from the 17th Summer Workshop on Hydraulic Engineering, B.1.1-B.1.16, 1981.

Kotoura, T., Kawasaki, K., Arikawa, T. and Akiyama, M.: Influence of resistance calculation method in numerical wave tank on wave force, *Journal of Japan Society of Civil Engineers, Ser.* B2 (Coastal Engineering), Vol.66, No1, pp.776-780, 2010.

Reinout, O., Augustijn, D., Wijnberg, K., Dekker, F. and Vries, M.: Modelling wave attenuation by vegetation with SWAN-VEG; Model evaluation and application to the Noordwaard polder, *Journal of Hydrology - J HYDROL*, 2010.

Tadokoro, A., Adi, P., Watanabe, M. and Arikawa, T.: Nu-merical Modeling of Tsunami Attenuation Effect with Mangrove, Journal of Japan Society of Civil Engineers, Ser. B2 (Coastal Engineering), Vol.77, Issue 2, pp. I_913-I_918, 2021.

Yanagisawa, H., Koshimura, S., Miyagi, T., Oie, T., Imamura, F., Potential Role of Mitigating Effects of Mangrove Forest against The 2004 Indian Ocean Tsunami in Banda Aceh, PROCEEDINGS OF COASTAL ENGINEERING, JSCE, pp.246-250, Vol.54, 2007.

Yanagisawa, H., Miyagi, T., Baba, S., Tsunami mitigation effect of mangrove forest in 2009 Samoa earthquake tsunami, Journal of Japan Society of Civil Engineers, Ser. B2 (Coastal Engineering), Volume 66, Issue 1, pp 251-255, 2010.

Yanagisawa, H., Yokoki, H., Mimura, N., T., Experimental and numerical investigation of wave attenuation by mangrove forests, *Journal of Japan Society of Civil Engineers, Ser.* B2 (Coastal Engineering), Vol.52, pp.1026-1030, 2005.

Yoshida, M., Shirai, T., Enomoto, Y. and Arikawa, T., Applicability of the dupuit-forchheimer law in reproducing wave height attenuation effects by mangroves, *Journal of Japan Society of Civil Engineers, Ser.* B2 (Coastal Engineering), Vol.79, No17,2023.